

Lag-correlated rising tones of electron cyclotron harmonic and whistler-mode upper-band chorus waves

Cite as: Phys. Plasmas **27**, 062903 (2020); <https://doi.org/10.1063/5.0008812>

Submitted: 25 March 2020 . Accepted: 29 May 2020 . Published Online: 23 June 2020

Zhonglei Gao , Xiongjun Shang , Pingbing Zuo , Zhengyang Zou , Geng Wang , Xueshang Feng , Yi Wang , Chunyi Guan, and Fengsi Wei

COLLECTIONS

 This paper was selected as Featured



[View Online](#)



[Export Citation](#)



[CrossMark](#)

ARTICLES YOU MAY BE INTERESTED IN

[Momentum-exchange current drive by electrostatic waves in an unmagnetized collisionless plasma](#)

[Physics of Plasmas](#) **27**, 062109 (2020); <https://doi.org/10.1063/5.0011516>

[Significant magnetospheric waves display surprising correlations](#)

[Scilight](#) **2020**, 261105 (2020); <https://doi.org/10.1063/10.0001516>

[A conservative approach to scaling magneto-inertial fusion concepts to larger pulsed-power drivers](#)

[Physics of Plasmas](#) **27**, 062707 (2020); <https://doi.org/10.1063/1.5135716>



NEW: TOPIC ALERTS

Explore the latest discoveries in your field of research

SIGN UP TODAY!



Lag-correlated rising tones of electron cyclotron harmonic and whistler-mode upper-band chorus waves



Cite as: Phys. Plasmas 27, 062903 (2020); doi: 10.1063/5.0008812

Submitted: 25 March 2020 · Accepted: 29 May 2020 ·

Published Online: 23 June 2020



View Online



Export Citation



CrossMark

Zhonglei Gao,^{1,2} Xiongjun Shang,² Pingbing Zuo,^{1,a)} Zhengyang Zou,¹ Geng Wang,¹ Xueshang Feng,¹ Yi Wang,¹ Chunyi Guan,² and Fengsi Wei¹

AFFILIATIONS

¹Institute of Space Science and Applied Technology, Harbin Institute of Technology, Shenzhen, Shenzhen 518055, China

²School of Physics and Electronic Sciences, Changsha University of Science and Technology, Changsha 410114, China

^{a)}Author to whom correspondence should be addressed: pbzuo@hit.edu.cn

ABSTRACT

Electron cyclotron harmonic (ECH) and whistler-mode chorus waves can contribute significantly to the magnetospheric dynamics. In the frequency-time spectrogram, ECH usually appears as a series of harmonic structureless bands, while chorus often exhibits successive discrete elements. Here, we present surprising observations by Van Allen Probes of lag-correlated rising tones of ECH and upper-band chorus waves. The time lags of ECH elements with respect to chorus elements range from 0.05 to 0.28 s, negatively correlated with the chorus peak amplitudes. The ECH elements seemingly emerge only when the chorus elements are sufficiently intense (peak amplitude $>3 \text{ mV m}^{-1}$), and their peak amplitudes are positively correlated. Our data and modeling suggest that upper-band chorus may promote the generation of ECH through rapidly precipitating the $\sim\text{keV}$ electrons near the loss cone. This phenomenon implies that ECH and chorus may not grow independently but competitively or collaboratively gain energy from hot electrons.

Published under license by AIP Publishing. <https://doi.org/10.1063/5.0008812>

I. INTRODUCTION

Electrostatic electron cyclotron harmonic (ECH) and electromagnetic whistler-mode chorus waves are frequently observed outside the plasmapause in the magnetosphere.^{1–5} Both ECH and chorus waves are able to cause auroral electron ($\sim\text{keV}$) precipitation.^{6–12} Chorus waves can contribute to the acceleration of radiation belt relativistic ($\sim\text{MeV}$) electrons.^{13–21} In the high-resolution frequency-time spectrogram, ECH waves usually appear as a series of harmonic structureless bands between $n f_{ce}$ and $(n+1)f_{ce}$ ($n = 1, 2, 3, \dots$ and f_{ce} is the equatorial electron gyrofrequency),^{22,23} while chorus waves often appear as successive discrete elements (e.g., rising, falling or even oscillating tones) below f_{ce} and are divided into the upper and lower bands by a gap around $0.5f_{ce}$.^{24–29}

ECH and chorus are believed to be excited by the loss cone instability and the temperature anisotropy instability of hot electrons, respectively.^{30–33} Their frequency distributions have been successfully explained by the linear instability theory.^{7,34,35} In addition, various nonlinear theories^{36–38} have been proposed to interpret the frequency sweeping structures of chorus. The instabilities of ECH and chorus are

usually treated as two independent wave-particle interaction processes, although their source electron populations have a significant overlap. Our recent study has reported the nonlinear coupling between chorus and ECH waves, which reveals an additional energy transfer process between them after their generation by hot electrons.³⁹ In this Letter, by analyzing Van Allen Probes data,⁴⁰ we present the first observations of lag-correlated rising tones of ECH and upper-band chorus waves. Our data and modeling suggest that upper-band chorus waves may trigger ECH waves via altering hot electron distributions.

II. DATA AND METHODS

The Van Allen Probes mission launched on 30 August 2012 is aimed to understand the fundamental physics of the Van Allen radiation belts.⁴⁰ We primarily use the data collected by the Electric Field and Wave (EFW) instrument,⁴¹ the Electric and Magnetic Field Instrument Suite and Integrated Science (EMFISIS) suite⁴² and the Energetic Particle, Composition, and Thermal Plasma (ECT) suite⁴³ onboard this mission. The EFW and EMFISIS together provide low-resolution DC electromagnetic fields for low-frequency wave modes

(e.g., ultralow frequency waves and magnetosonic waves) and high-resolution AC waveforms for high frequency wave modes (e.g., whistler and ECH waves). The low-resolution magnetic fields with a 64 Hz sampling rate are observed by the tri-axial flux gate magnetometer (MAG) of the EMFISIS suite, and are transformed into a mean field aligned (MFA) coordinate system. The low-resolution electric fields at 32 samples/s are observed by the EFW in an mGSE (modified GSE) coordinate system. Because only the two components of electric fields in the spin plane are available, we just use them in the mGSE coordinate system directly. The continuous burst-mode waveforms consisting of the electromagnetic components in the spacecraft science (UVW) coordinate system are provided by the Waveform Receiver (WFR) of the EMFISIS wave instrument, and each waveform data block lasts for about 6 s with a 35 kHz sampling rate. A 1024-point fast Fourier transform is applied on these high frequency waveforms to obtain the wave spectral matrices. The wave Poynting fluxes are calculated from the cross-power spectra between electric and magnetic components.⁴⁴ The singular value decomposition technique⁴⁵ is adopted on the spectral matrices to estimate the wave normal angles and determine the magnetic polarizations. The cold electron density is inferred from the upper hybrid resonance frequency detected by the High Frequency Receiver (HFR) of the EMFISIS Waves instrument.⁴⁶ The equatorial magnetic field is estimated by substituting the local geomagnetic field measurement into the TS04 model,⁴⁷ thus the equatorial electron gyrofrequency is obtained. The electron fluxes at energies 15 eV–3.8 MeV are from the Helium, Oxygen, Proton, and Electron (HOPE) Mass Spectrometer⁴⁸ and the Magnetic Electron Ion Spectrometer (MagEIS)⁴⁹ of the ECT suite.⁴³

III. OBSERVATIONS

Figure 1 presents two wave events observed by Van Allen Probe B in the burst-mode. For the first event around 01:55 UT on 06 September 2014, the probe was in the dawnside (MLT = 5.1) equatorial (MLAT = 4.6) plasma trough ($L = 6.1$). There were electromagnetic upper-band chorus rising tones repeating at a period of ~ 1 s in the frequency range of 0.5–0.8 f_{ce} . These chorus elements propagated quasi-parallel to the background magnetic fields and possessed right-hand circular polarizations. Four electrostatic wave bands occurred above the frequency f_{ce} . All these electrostatic bands were composed of intermittent rising tones which slightly lagged behind the chorus rising tones. The two relatively intense electrostatic bands with the frequencies between the harmonics of f_{ce} are considered the first and second ECH. In Fig. 2(c), we use the power-weighted center frequencies rather than the peak power frequencies to represent the frequencies of the chorus (f_c , black lines) and the first and second ECH bands (f_{E1} and f_{E2} , white lines), since the frequency ranges of the ECH bands were pretty wide and the peak power frequencies oscillated significantly. The frequency profiles of the other two weak electrostatic bands are well characterized by $f_c + f_{E1}$ (red lines), $f_c + f_{E2}$ (green lines), and $f_{E2} - f_c$ (orange lines), indicating that they were ECH sidebands produced by the nonlinear interactions between the rising tones of ECH and chorus waves.³⁹ At a similar spatial location, the second event occurred around 21:53 UT on 18 September 2014. One major difference of the second event from the first event is the occurrence of typical structureless ECH bands with nearly constant frequencies. Lag-correlated rising tones of ECH and upper-band chorus waves as well as an ECH sideband produced by the nonlinear wave-wave

interactions [Fig. 2(f)] emerged once again. As shown in Fig. 2, these intermittent elements of both events were not modulated by ultralow frequency waves,^{50–52} whose repetition was likely a manifestation of the natural plasma instabilities. Because the observation locations of the probes were close to the equatorial wave source region, the frequency sweeping characteristics of these rising tones were unlikely to be a consequence of the propagation effect.

Checking the other nearby burst-mode data blocks of the 06 September 2014 event (e.g., Fig. 3), we find that the ECH rising tones disappeared when the upper-band chorus rising tones became weak. With 5 burst-mode data blocks from 01:54:50 to 01:55:21 UT on 06 September 2014 (not shown), we plot the relation between the peak amplitudes of the ECH and upper-band chorus ring tones [Fig. 4(b)]. The ECH rising tones occurred only when the chorus peak amplitudes exceeded ~ 3 mV m⁻¹, and their peak amplitudes were positively correlated (with correlation coefficients of 0.83). For the five burst-mode data blocks, we define the start time of each rising tone as the time when its amplitude exceeded a threshold, and then calculate the time lags between the ECH and chorus ring tones [an example of a data block shown in Fig. 4(a)]. The thresholds are selected to avoid the interference of noises and to effectively isolate the rising tone signatures, altering the thresholds will not qualitatively change the conclusion. As shown in Fig. 4(c), the time lags ranged from 0.05 to 0.28 and seemed to be negatively correlated (with correlation coefficients of -0.69 and -0.61) with the chorus peak amplitudes. For the 18 September 2014 event, the burst-mode data block shown in Fig. 1 is the only one recorded. Similarly, a threshold (~ 4 mV m⁻¹) of the upper-band chorus waves for the generation of the ECH waves and a positive correlation between their peak amplitudes can still be identified [with correlation coefficients of 0.42 and 0.55, Fig. 4(e)]. Probably because of the limited data points, the potential relation between the time lags and the chorus amplitudes is unclear [with correlation coefficients of -0.2 and -0.13 , Fig. 4(f)].

IV. DISCUSSIONS

The ECH rising tones presented in this Letter are a novel phenomenon different from the typical ECH structureless bands. Here, we take the 06 September 2014 event as an example and qualitatively investigate the generation of such ECH rising tones in the linear instability framework. The linear growth rates of ECH waves are calculated using the Waves in Homogeneous Anisotropic Magnetized Plasma (WHAMP) code.⁵³ The electron phase space density is expressed as a sum of subtracted Maxwellian distributions³⁰

$$F = \sum_{i=1}^N F_i = \sum_{i=1}^N \frac{n_i}{(\sqrt{\pi} V_{thi})^3} \exp\left(-\frac{v_{||}^2}{V_{thi}^2}\right) \times \left\{ \frac{\Delta_i}{\alpha_i} \exp\left(-\frac{v_{\perp}^2}{\alpha_i V_{thi}^2}\right) + \frac{1 - \Delta_i}{\alpha_i - \beta_i} \left[\exp\left(-\frac{v_{\perp}^2}{\alpha_i V_{thi}^2}\right) - \exp\left(-\frac{v_{\perp}^2}{\beta_i V_{thi}^2}\right) \right] \right\}, \quad (1)$$

where N is the number of plasma components; for the i th plasma component, n_i and $V_{thi} = \sqrt{2T_i/m_e}$ represent the density and parallel thermal velocity, T_i and α_i denote the parallel temperature and temperature anisotropy, and β_i and Δ_i characterize the size and depth of the loss cone feature. For this event, a combination of $N=4$

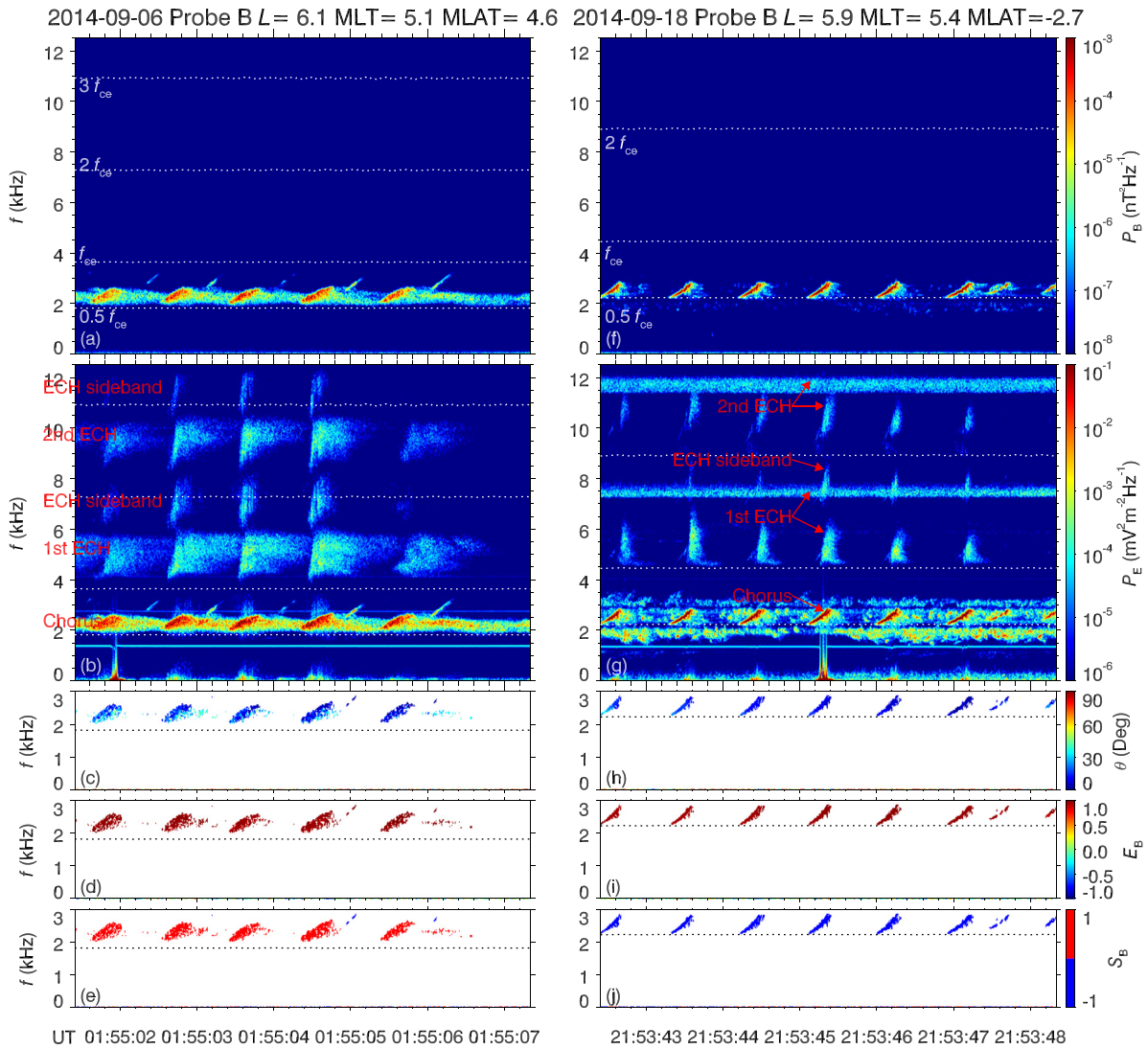


FIG. 1. Wave power, propagation, and polarization information of the events on 06 September 2014 (left) and 18 September 2014 (right): [(a) and (f)] magnetic and [(b) and (g)] electric power spectral densities P_B and P_E , [(c) and (h)] wave normal angles θ , [(d) and (i)] magnetic ellipticities E_B , and [(e) and (j)] signs S_B of Poynting fluxes parallel to the background magnetic field. The dotted lines represent $0.5f_{ce}$, f_{ce} , $2f_{ce}$, and $3f_{ce}$, respectively.

components is sufficient to well reproduce the observed electron distribution in the energy range of interest (Table I and Fig. 5). The available electron flux data have two shortcomings: (1) a much longer acquisition time of each data frame > 10 s than the duration of the wave discrete element < 1 s, and (2) data gaps near the loss cone, where ECH waves mainly gain energies from ~ 1 keV electrons.^{7,10,31} Therefore, we parametrically investigate the dependence of wave frequency on the loss cone feature parameters Δ_3 and β_3 of the third component with $T_3 = 0.182$ keV, which dominate the distribution of ECH source electrons (hundreds eV to ~ 1 keV). Note that the changes of Δ_3 and β_3 do not represent the variation of the “loss cone angle” determined by the background magnetic field geometry, but merely modify the electron distributions near the loss cone. We introduce the root mean square relative error σ to evaluate the goodness of fit

$$\sigma = \sqrt{\frac{1}{M} \sum_{j=1}^M \left(\frac{F_j^{obs} - F_j^{fit}}{F_j^{fit}} \right)^2}, \quad (2)$$

with the observed phase space density F_j^{obs} and the fitted phase space density F_j^{fit} . Since there is little difference among the six fitting cases in the observable region (pitch angle $> 18^\circ$), all the σ values are close to 0.25. If F_j^{fit} is replaced by the observed phase space densities at the two adjacent time points, their σ values would reach 0.47–0.77. Given the obvious temporal fluctuations of data, our fitting seems to be acceptable. As shown in Fig. 6, the decrease in Δ_3 mainly reduces the parallel ($< 4^\circ$) phase space densities, while the increase in β_3 causes the steep decrease in phase space densities to emerge at higher pitch angles (up to $\sim 13^\circ$). The changes of Δ_3 have little effect on the instability

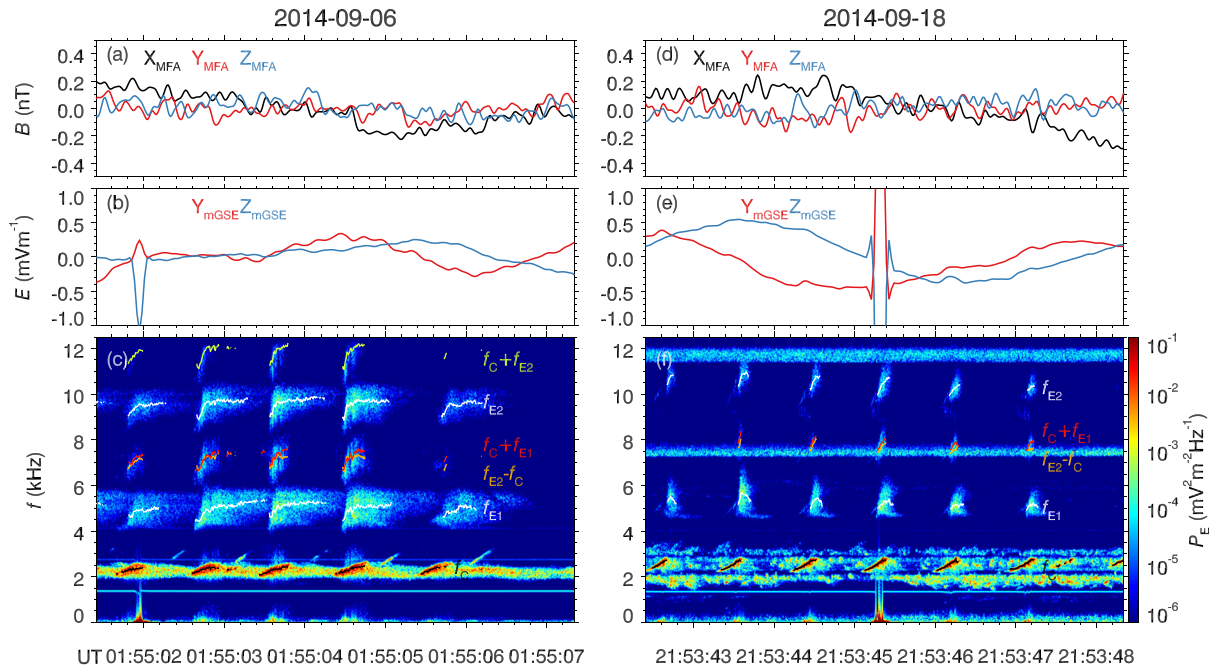


FIG. 2. [(a), (b), (d), and (e)] Low frequency electromagnetic B and E fields and [(c) and (f)] high frequency wave spectra P_E for the 06 September 2014 event (left) and 18 September 2014 events (right). The low frequency electromagnetic fields are detrended and low-pass filtered over <7 Hz. The f_C (black lines), f_{E1} and f_{E2} (white lines) represent the power-weighted frequencies of the chorus, the first ECH band, and the second ECH band, respectively, which are calculated using the equation $\frac{\sum_{f_c}^{f_{uc}} P_E(f)f}{\sum_{f_c}^{f_{uc}} P_E(f)}$, with the upper frequency cutoff f_{uc} and the lower frequency cutoff f_{lc} of each wave band. $f_C + f_{E1}$ (red lines), $f_C + f_{E2}$ (green lines), and $f_{E2} - f_C$ (orange lines) are plotted in Figs. 2(c) and 2(f).

frequency range [Figs. 5(a)–5(f)], but the increase in β_3 moves the ECH wave frequencies with the maximum growth rates from $<(n+0.2)f_{ce}$ to $>(n+0.4)f_{ce}$ [Figs. 5(g)–5(l)]. This frequency variation is comparable to the observed frequency sweeping of ECH rising tones [Fig. 1(b)]. These calculations suggest that, under the linear instability assumption, the expansion of the loss cone feature is a candidate mechanism for the generation of ECH rising tones.

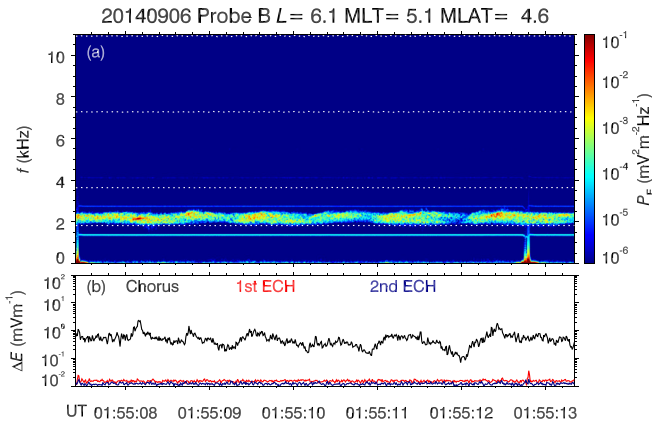


FIG. 3. The electric wave (a) spectra P_E and (b) amplitudes ΔE recorded by the burst-mode data block next to that of the left column of Fig. 1.

Considering the lag-correlation between the ECH and chorus rising tones, we speculate that the intense upper-band chorus waves may have the ability to trigger the ECH waves through altering the hot electron distributions. Figure 7 plots the minimum electron cyclotron and Landau resonant energies of whistler-mode waves. The source electrons of ECH waves are approximately in the energy range from hundreds eV to ~ 1 keV. For cyclotron resonance, the upper-band chorus can effectively interact with the $\lesssim 1$ keV electrons; for Landau resonance, both upper- and lower-band chorus waves have to interact with $\gtrsim 1$ keV electrons. Hence, we speculate that the cyclotron resonance between the upper-band chorus waves and electrons contribute dominantly to the excitation of ECH waves. This is also consistent with that ECH rising tones always follow upper-band chorus waves. The possible scenario is described as follows: (1) the initial electron distribution is unstable for chorus but stable for ECH; (2) a upper-band chorus rising tone grows, gradually transports hot electrons into the loss cone through the cyclotron resonance,^{7,8,10,54} reduces the phase space densities at higher pitch angles (up to $\sim 13^\circ$ according to our estimate) and thus affects the parameter β ; (3) the disturbed electron distribution becomes unstable for ECH waves and a gradual loss of electrons corresponds to a gradual increase in the ECH wave frequency; and (4) after the termination of the chorus rising tone, enough inflow of fresh electrons causes the instabilities to restart. This scenario is composed of two successive wave-particle interactions: (1) upper-band chorus-electron interaction and (2) ECH-electron interaction. This scenario is essentially different from the nonlinear three-wave

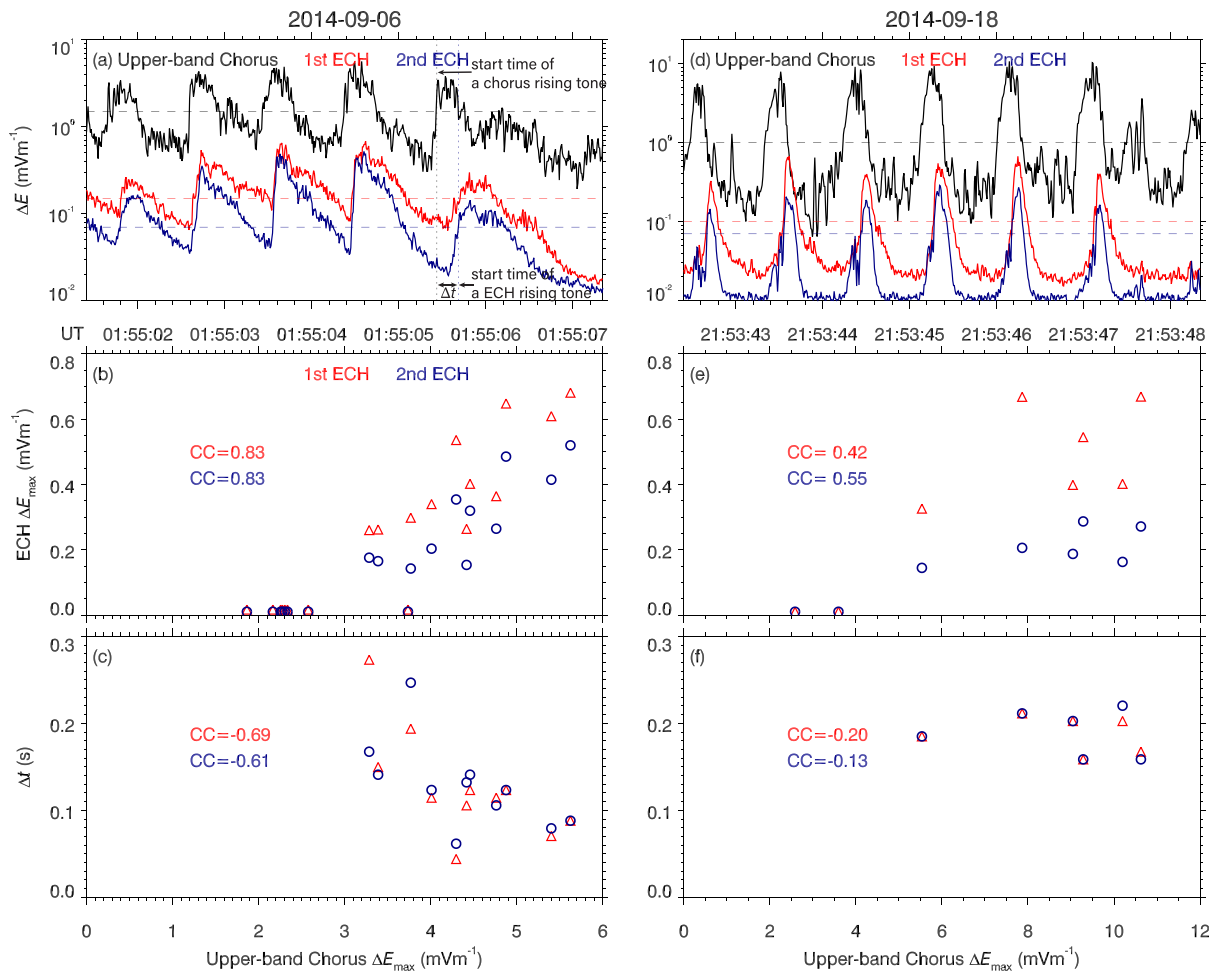


FIG. 4. The relation between the upper-band chorus (black) and ECH (red for the first harmonic and blue for the second harmonic) waves of the 06 September 2014 event (left) and the 18 September 2014 event (right): [(a) and (d)] wave amplitude series ΔE of the upper-band chorus and two ECH bands recorded by the date blocks shown in Fig. 1, the [(b) and (e)] peak amplitudes ΔE_{\max} and [(c) and (f)] time lags Δt of the ECH rising tones as functions of the peak amplitudes ΔE_{\max} of the corresponding upper-band chorus rising tones. The horizontal dashed lines in Figs. 4(a) and 4(d) represent the amplitude thresholds used to determine the start times of the rising tones, and the vertical dotted lines in Fig. 4(a) express how the time lags Δt between the ECH and upper-band chorus rising tones are calculated for the two events. The ΔE_{\max} and Δt of the 06 September 2014 event are obtained from the data in Fig. 4(a) and the other 4 nearby burst-mode data blocks from 01:54:50 to 01:55:21 UT, and those of the 18 September 2014 event are from the data in Fig. 4(d). In Figs. 4(b)–4(f), the correlation coefficients (CC) between those quantities and upper-band chorus peak amplitudes ΔE_{\max} are listed.

coupling, which produces ECH sidebands from the rising tones of ECH and chorus waves.³⁹

Because the chorus wave with a larger amplitude can scatter the electrons more rapidly, the time lags between the ECH and chorus rising tones tend to be negatively correlated with the chorus amplitudes

[Fig. 4(c)]. The $\sim 3 \text{ mV m}^{-1}$ amplitude threshold of chorus waves for the generation of ECH [Fig. 4(b)] may be interpreted as that a weak chorus element cannot produce an effective loss cone distribution under the competition with the fresh electron inflow. Stronger chorus waves may imply more abundant free energy of the system and can be expected to trigger stronger ECH waves. As shown by Figs. 5 and 6, a $\sim 30\%$ reduction of phase space densities at small pitch angles is required to product such a ECH rising tone. Whether the chorus can alter the distribution in such a short time scale (0.1–0.3 s) should be examined in the future.

V. SUMMARY

For understanding the magnetospheric electron dynamic, the knowledge of the generation of electron cyclotron harmonic (ECH) and whistler-mode chorus waves is required. In the past, various linear

TABLE I. Fitting parameters for electron phase space density.

Component	$n_i (\text{m}^{-3})$	$T_i (\text{keV})$	α_i	Δ_i	β_i
1	2.79×10^6	0.009	0.69	1	0
2	0.5×10^6	0.021	2.20	1	0
3	1.2×10^5	0.182	1.50	Listed in Fig. 5	
4	0.9×10^5	2.07	1.40	0.5	0.56

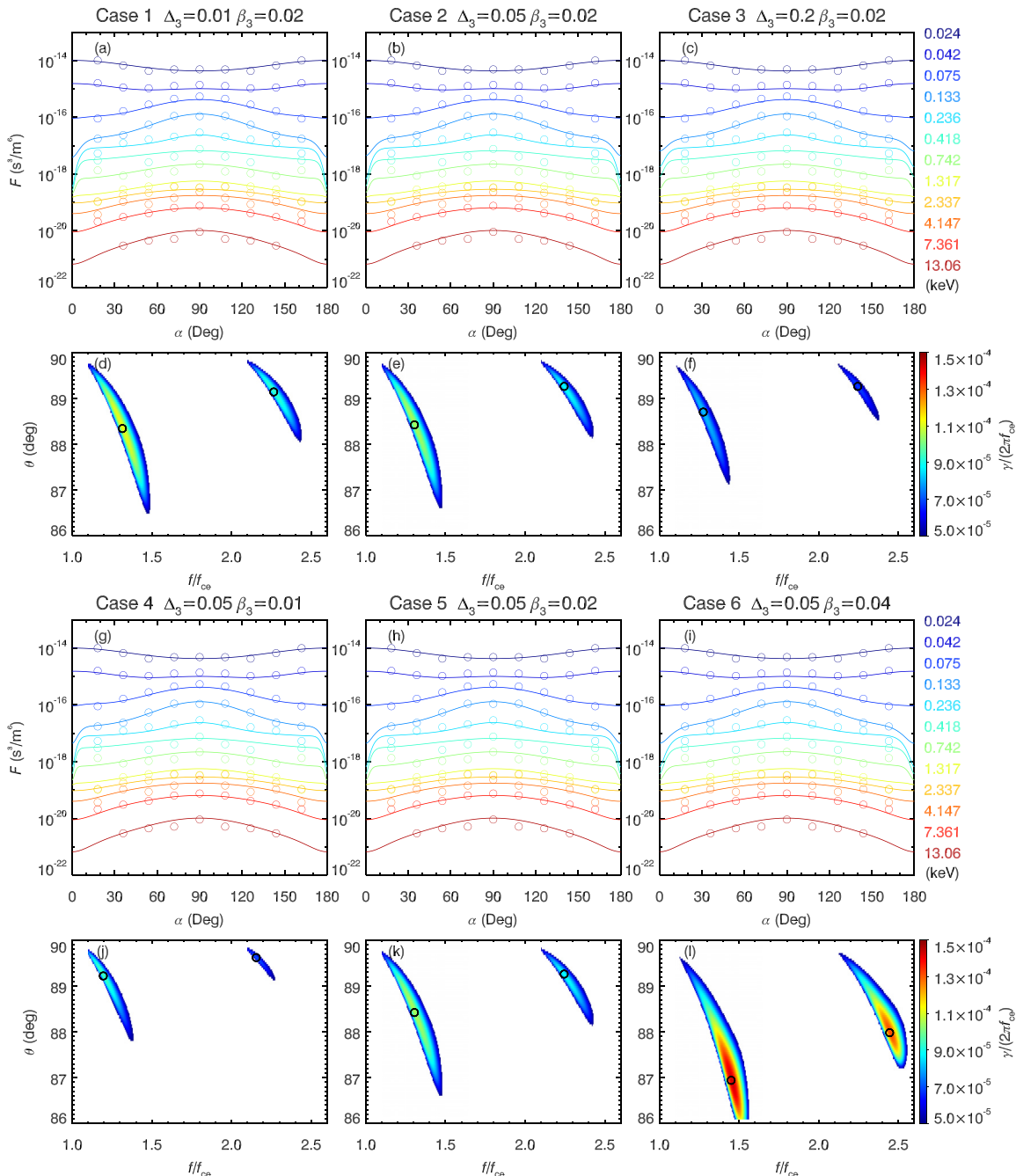


FIG. 5. Six cases of [(a), (b), (c), (g), (h), and (i)] modeled (lines) and observed (circles) electron phase space density F as functions of pitch angle α at selected energies (represented by different colors), and [(d), (e), (f), (j), (k), and (l)] their corresponding growth rates γ of the ECH wave in the frequency f/f_{ce} —normal angle θ domain. The common fitting parameters for the six modeled distributions are listed in Table I, the private fitting parameters Δ_3 and β_3 for their own are listed in the figure. The circles in Figs. 5(d)–5(f) and 5(j)–5(l) mark the peak growth rates.

and nonlinear instability theories have been proposed to explain their frequency-time structures.^{7,30–32,36–38} The generations of the two types of waves were usually treated as two independent wave-particle interaction processes, although their source electron populations have a

significant overlap. By analyzing Van Allen Probes data, we present the novel observations of lag-correlated rising tones of ECH and upper-band chorus waves. The ECH elements tend to follow the chorus elements with large enough ($>3 \text{ mV m}^{-1}$) peak amplitudes, and

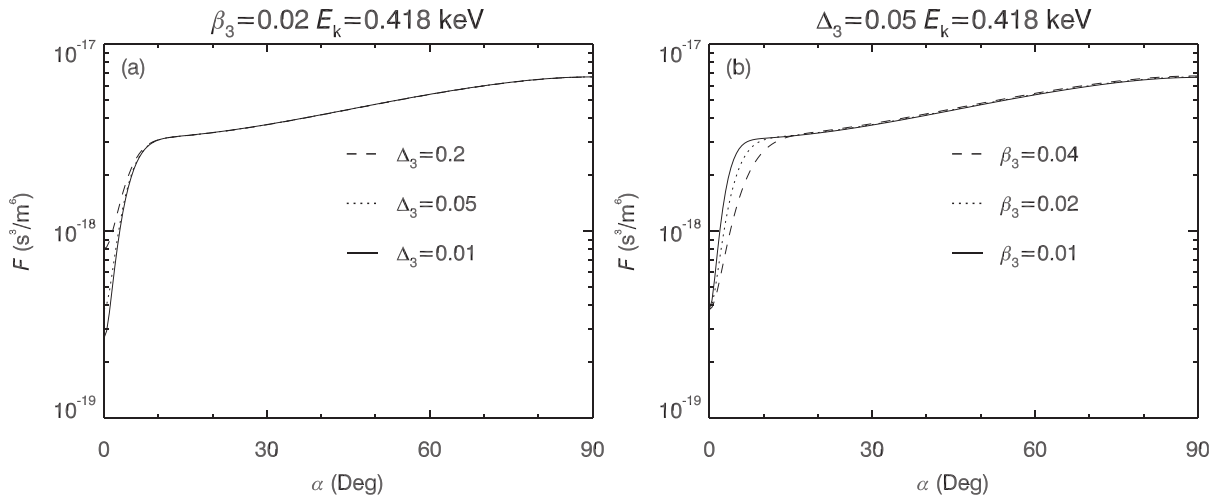


FIG. 6. Modeled electron phase space density F as functions of pitch angle α at 0.418 keV: (a) F taken from Figs. 5(a)–5(c) and (b) F taken from Figs. 5(g)–5(i).

their time lags (0.05–0.28 s) seem to be negatively correlated with the chorus peak amplitudes. Our linear instability calculations show that the ECH instability frequency range is mainly controlled by the size of the \sim keV electron loss cone feature. On the basis of observations and simulations, we suggest that upper-band chorus waves may trigger ECH waves through rapidly precipitating the \sim keV electrons near the loss cone. Our present findings, together with the previous study about the nonlinear ECH-chorus interactions,³⁹ highlight the complex interplay between ECH and chorus instabilities in the magnetospheric plasma.

We reiterate that ECH waves usually appear as structureless bands in the frequency-time spectrogram. Whether or not there is any relation between the typical structureless ECH waves and upper-band chorus waves remains unclear. Our present study is limited to the small sample size (four blocks of burst-mode data on 6 and 8 September 2014) and the lack of self-consistent, quantitative examination of the proposed scenario. In the future, more statistical, theoretical, and numerical studies are required to understand the potential interplay between ECH and chorus instabilities.

ACKNOWLEDGMENTS

This work was supported by the National Natural Science Foundation of China (Grant Nos. 41731067, 41804171, 41822404, and 41974212), the China Postdoctoral Science Foundation (Grant No. 2019M661263), the Guangdong Basic and Applied Basic Research Foundation (Grant No. 2019A1515011067), and the Shenzhen Technology Project (Grant No. JCYJ20180306171748011). The present work was also partially supported by the B-type Strategic Priority Program of the Chinese Academy of Sciences (Grant No. XDB41000000).

DATA AVAILABILITY

The data that support the findings of this study are openly available in EFW at <http://www.space.umn.edu/rbspefw-data/>, Ref. 41; EMFSIS at <http://emfisis.physics.uiowa.edu/Flight/>, Ref. 42; and ECT <http://www.rbsp-ect.lanl.gov/>, Ref. 43.

REFERENCES

- ¹C. F. Kennel and H. E. Petschek, *J. Geophys. Res.* **71**, 1, <https://doi.org/10.1029/JZ071i001p00001> (1966).
- ²R. B. Horne, P. J. Christiansen, M. P. Gough, K. G. Ronnmark, J. F. E. Johnson, J. Sojka, and G. L. Wrenn, *Nature* **294**, 338 (1981).
- ³N. P. Meredith, R. B. Horne, R. M. Thorne, and R. R. Anderson, *J. Geophys. Res.* **114**, A07218, <https://doi.org/10.1029/2008JA013889> (2009).

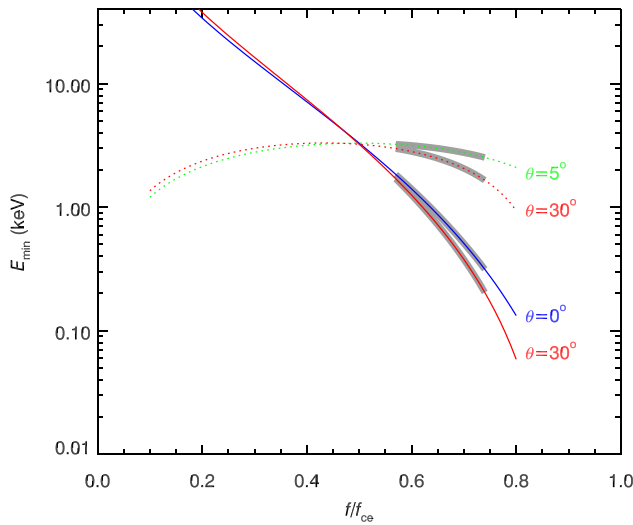


FIG. 7. Minimum electron energy E_{\min} as a function of normalized frequency f/f_{ce} for the cyclotron (solid lines) and Landau (dotted lines) resonances with the whistler-mode wave for the 06 September 2014 event, with shadows denoting the observed upper-band chorus waves. The lines are color-coded according to normal angles θ .

- ⁴F. Xiao, C. Yang, Z. Su, Q. Zhou, Z. He, Y. He, D. Baker, H. Spence, H. Funsten, and J. Blake, *Nat. Commun.* **6**, 8590 (2015).
- ⁵B. Ni, X. Gu, S. Fu, Z. Xiang, and Y. Lou, *J. Geophys. Res.* **122**, 3342, <https://doi.org/10.1002/2016JA023433> (2017).
- ⁶L. R. Lyons, *J. Geophys. Res.* **79**, 575, <https://doi.org/10.1029/JA079i004p00575> (1974).
- ⁷R. B. Horne, R. M. Thorne, N. P. Meredith, and R. R. Anderson, *J. Geophys. Res.* **108**, 1290, <https://doi.org/10.1029/2002JA009736> (2003).
- ⁸Z. Su, H. Zheng, and S. Wang, *J. Geophys. Res.* **115**, A05219, <https://doi.org/10.1029/2009JA014759> (2010).
- ⁹Z. Su, H. Zheng, and S. Wang, *J. Geophys. Res.* **114**, A08202, <https://doi.org/10.1029/2009JA014269> (2009).
- ¹⁰R. M. Thorne, B. Ni, X. Tao, R. B. Horne, and N. P. Meredith, *Nature* **467**, 943 (2010).
- ¹¹Y. Nishimura, J. Bortnik, W. Li, R. M. Thorne, L. R. Lyons, V. Angelopoulos, S. B. Mende, J. W. Bonnell, O. L. Contel, C. Cully, R. Ergun, and U. Auster, *Science* **330**, 81 (2010).
- ¹²B. Ni, R. Thorne, J. Liang, V. Angelopoulos, C. Cully, W. Li, X. Zhang, M. Hartinger, O. Le Contel, and A. Roux, *Geophys. Res. Lett.* **38**, L17105 (2011).
- ¹³D. Summers, R. M. Thorne, and F. Xiao, *J. Geophys. Res.* **103**, 20487, <https://doi.org/10.1029/98JA01740> (1998).
- ¹⁴R. M. Thorne, W. Li, B. Ni, Q. Ma, J. Bortnik, L. Chen, D. N. Baker, H. E. Spence, G. D. Reeves, M. G. Henderson, C. A. Kletzing, W. S. Kurth, G. B. Hospodarsky, J. B. Blake, J. F. Fennell, S. G. Claudepierre, and S. G. Kanekal, *Nature* **504**, 411 (2013).
- ¹⁵Z. Su, F. Xiao, H. Zheng, Z. He, H. Zhu, M. Zhang, C. Shen, Y. Wang, S. Wang, C. A. Kletzing, W. S. Kurth, G. B. Hospodarsky, H. E. Spence, G. D. Reeves, H. O. Funsten, J. B. Blake, and D. N. Baker, *Geophys. Res. Lett.* **41**, 229, <https://doi.org/10.1002/2013GL058912> (2014).
- ¹⁶Y. Y. Shprits, R. M. Thorne, R. B. Horne, S. A. Glauert, M. Cartwright, C. T. Russell, D. N. Baker, and S. G. Kanekal, *Geophys. Res. Lett.* **33**, L05104 (2006).
- ¹⁷F. Xiao, Z. Su, H. Zheng, and S. Wang, *J. Geophys. Res.* **115**, A05216 (2010).
- ¹⁸S. Liu, F. Xiao, C. Yang, Y. He, Q. Zhou, C. A. Kletzing, W. S. Kurth, G. B. Hospodarsky, H. E. Spence, G. D. Reeves, H. O. Funsten, J. B. Blake, D. N. Baker, and J. R. Wygant, *J. Geophys. Res.* **120**, 938, <https://doi.org/10.1002/2014JA020781> (2015).
- ¹⁹L. Li, J. Cao, and G. Zhou, *J. Geophys. Res.* **110**, A03203 (2005).
- ²⁰L. Y. Li, J. Yu, J. B. Cao, J. Y. Yang, X. Li, D. N. Baker, G. D. Reeves, and H. E. Spence, *J. Geophys. Res.* **122**, 5431, <https://doi.org/10.1002/2016JA023634> (2017).
- ²¹J. Yu, L. Li, J. Cui, J. Cao, and J. Wang, *Geophys. Res. Lett.* **46**, 8624, <https://doi.org/10.1029/2019GL084004> (2019).
- ²²C. F. Kennel, F. L. Scarf, R. W. Fredricks, J. H. McGehee, and F. V. Coroniti, *J. Geophys. Res.* **75**, 6136, <https://doi.org/10.1029/JA075i031p06136> (1970).
- ²³R. W. Fredricks and F. L. Scarf, *J. Geophys. Res.* **78**, 310, <https://doi.org/10.1029/JA078i001p00310> (1973).
- ²⁴B. T. Tsurutani and E. J. Smith, *J. Geophys. Res.* **79**, 118, <https://doi.org/10.1029/JA079i001p00118> (1974).
- ²⁵W. J. Burtis and R. A. Helliwell, *Planet. Space Sci.* **24**, 1007 (1976).
- ²⁶O. Santolik, D. A. Gurnett, J. S. Pickett, M. Parrot, and N. Cornilleau-Wehrlin, *J. Geophys. Res.* **108**, 1278, <https://doi.org/10.1029/2002JA009791> (2003).
- ²⁷H. S. Fu, J. B. Cao, C. M. Cully, Y. V. Khotyaintsev, A. Vaivads, V. Angelopoulos, Q.-G. Zong, O. Santolik, E. Macúšová, M. André, W. L. Liu, H. Y. Lu, M. Zhou, S. Y. Huang, and Z. Zhima, *J. Geophys. Res.* **119**, 9089, <https://doi.org/10.1002/2014JA020204> (2014).
- ²⁸Z. Gao, Z. Su, L. Chen, H. Zheng, Y. Wang, and S. Wang, *Geophys. Res. Lett.* **44**, 5909, <https://doi.org/10.1002/2017GL073420> (2017).
- ²⁹J. Yu, L. Y. Li, J. Cui, and J. Wang, *J. Geophys. Res.* **123**, 6670, <https://doi.org/10.1029/2018JA025875> (2018).
- ³⁰M. Ashour-Abdalla and C. F. Kennel, *J. Geophys. Res.* **83**, 1531, <https://doi.org/10.1029/JA083iA04p01531> (1978).
- ³¹R. B. Horne and R. M. Thorne, *J. Geophys. Res.* **105**, 5391, <https://doi.org/10.1029/1999JA900447> (2000).
- ³²F. Xiao, Q. Zhou, H. Zheng, and S. Wang, *J. Geophys. Res.* **111**, A08208, <https://doi.org/10.1029/2006JA011612> (2006).
- ³³Q. Zhou, F. Xiao, C. Yang, S. Liu, Y. He, D. Baker, H. Spence, G. D. Reeves, and H. O. Funsten, *Geophys. Res. Lett.* **44**, 5251, <https://doi.org/10.1002/2017GL073051> (2017).
- ³⁴Z. Su, H. Zhu, F. Xiao, H. Zheng, Y. Wang, Z. He, C. Shen, C. Shen, C. B. Wang, R. Liu, M. Zhang, S. Wang, C. A. Kletzing, W. S. Kurth, G. B. Hospodarsky, H. E. Spence, G. D. Reeves, H. O. Funsten, J. B. Blake, D. N. Baker, and J. R. Wygant, *J. Geophys. Res.* **119**, 4266, <https://doi.org/10.1002/2014JA019919> (2014).
- ³⁵Q. Zhou, C. Yang, Y. He, S. Liu, Z. Gao, and F. Xiao, *Geophys. Res. Lett.* **46**, 1929, <https://doi.org/10.1029/2018GL081379> (2019).
- ³⁶D. Nunn, Y. Omura, H. Matsumoto, I. Nagano, and S. Yagitani, *J. Geophys. Res.* **102**, 27083, <https://doi.org/10.1029/97JA02518> (1997).
- ³⁷Y. Omura, Y. Katoh, and D. Summers, *J. Geophys. Res.* **113**, A04223 (2008).
- ³⁸X. Tao, *J. Geophys. Res.* **119**, 3362, <https://doi.org/10.1002/2014JA019820> (2014).
- ³⁹Z. Gao, Z. Su, F. Xiao, D. Summers, N. Liu, H. Zheng, Y. Wang, F. Wei, and S. Wang, *Geophys. Res. Lett.* **45**, 12,685, <https://doi.org/10.1029/2018GL080635> (2018).
- ⁴⁰B. H. Mauk, N. J. Fox, S. G. Kanekal, R. L. Kessel, D. G. Sibeck, and A. Ukhorskiy, *Space Sci. Rev.* **179**, 3 (2013).
- ⁴¹J. Wygant, J. Bonnell, K. Goetz, R. Ergun, F. Mozer, S. Bale, M. Ludlam, P. Turin, P. Harvey, R. Hochmann, K. Harps, G. Dalton, J. McCauley, W. Rachelson, D. Gordon, B. Donakowski, C. Shultz, C. Smith, M. Diaz-Aguado, J. Fischer, S. Heavner, P. Berg, D. Malsapina, M. Bolton, M. Hudson, R. Strangeway, D. Baker, X. Li, J. Albert, J. Foster, C. Chaston, I. Mann, E. Donovan, C. Cully, C. Cattell, V. Krasnoselskikh, K. Kersten, A. Brenneman, and J. Tao, *Space Sci. Rev.* **179**, 183 (2013).
- ⁴²C. A. Kletzing, W. S. Kurth, M. Acuna, R. J. MacDowell, R. B. Torbert, T. Averkamp, D. Bodet, S. R. Bounds, M. Chutter, J. Connerney, D. Crawford, J. S. Dolan, R. Dvorsky, G. B. Hospodarsky, J. Howard, V. Jordanova, R. A. Johnson, D. L. Kirchner, B. Mokrzycki, G. Needell, J. Odom, D. Mark, R. Pfaff, J. R. Phillips, C. W. Piker, S. L. Remington, D. Rowland, O. Santolik, R. Schnurr, D. Sheppard, C. W. Smith, R. M. Thorne, and J. Tyler, *Space Sci. Rev.* **179**, 127 (2013).
- ⁴³H. E. Spence, G. D. Reeves, D. N. Baker, J. B. Blake, M. Bolton, S. Bourdarie, A. H. Chan, S. G. Claudepierre, J. H. Clemmons, J. P. Cravens, S. R. Elkington, J. F. Fennell, R. H. W. Friedel, H. O. Funsten, J. Goldstein, J. C. Green, A. Guthrie, M. G. Henderson, R. B. Horne, M. K. Hudson, J.-M. Jahn, V. K. Jordanova, S. G. Kanekal, B. W. Klatt, B. A. Larsen, X. Li, E. A. MacDonald, I. R. Mann, J. Niehof, T. P. O'Brien, T. G. Onsager, D. Salvaggio, R. M. Skoug, S. S. Smith, L. L. Suther, M. F. Thomsen, and R. M. Thorne, *Space Sci. Rev.* **179**, 311 (2013).
- ⁴⁴O. Santolik, J. S. Pickett, D. A. Gurnett, J. D. Menietti, B. T. Tsurutani, and O. Verkhoglyadova, *J. Geophys. Res.* **115**, 1, <https://doi.org/10.1029/2009JA014925> (2010).
- ⁴⁵O. Santolik, M. Parrot, and F. Lefevre, *Radio Sci.* **38**, 1010 (2003).
- ⁴⁶W. S. Kurth, S. D. Pascuale, J. B. Faden, C. A. Kletzing, G. B. Hospodarsky, S. Thaller, and J. R. Wygant, *J. Geophys. Res.* **120**, 904, <https://doi.org/10.1002/2014JA020857> (2015).
- ⁴⁷N. A. Tsyganenko and M. I. Sitnov, *J. Geophys. Res.* **110**, A03208, <https://doi.org/10.1029/2004JA010798> (2005).
- ⁴⁸H. O. Funsten, R. M. Skoug, A. A. Guthrie, E. A. MacDonald, J. R. Baldonado, R. W. Harper, K. C. Henderson, K. H. Kihara, J. E. Lake, B. A. Larsen, A. D. Puckett, V. J. Vigil, R. H. Friedel, M. G. Henderson, J. T. Niehof, G. D. Reeves, M. F. Thomsen, J. H. Hanley, D. E. George, J.-M. Jahn, S. Cortinas, A. De Los Santos, G. Dunn, E. Edlund, M. Ferris, M. Freeman, M. Maple, C. Nunez, T. Taylor, W. Tocynski, C. Urdiales, H. E. Spence, J. A. Cravens, L. L. Suther, and J. Chen, *Space Sci. Rev.* **179**, 423 (2013).
- ⁴⁹J. B. Blake, P. A. Carranza, S. G. Claudepierre, J. H. Clemmons, W. R. Crain, Y. Dotan, J. F. Fennell, F. H. Fuentes, R. M. Galvan, J. S. George, M. G. Henderson, M. Lalic, A. Y. Lin, M. D. Looper, D. J. Mabry, J. E. Mazur, B. McCarthy, C. Q. Nguyen, T. P. O'Brien, M. A. Perez, M. T. Redding, J. L. Roeder, D. J. Salvaggio, G. A. Sorensen, H. E. Spence, S. Yi, and M. P. Zakrzewski, *Space Sci. Rev.* **179**, 383 (2013).
- ⁵⁰W. Li, R. M. Thorne, J. Bortnik, Y. Nishimura, and V. Angelopoulos, *J. Geophys. Res.* **116**, A06205 (2011).

⁵¹C. A. Colpitts, C. A. Cattell, M. Engebretson, M. Broughton, S. Tian, J. Wygant, A. Breneman, and S. Thaller, *Geophys. Res. Lett.* **43**, 11,510, <https://doi.org/10.1002/2016GL071566> (2016).

⁵²X. J. Zhang, L. Chen, A. V. Artemyev, V. Angelopoulos, and X. Liu, *J. Geophys. Res.* **124**, 8535, <https://doi.org/10.1029/2019JA027201> (2019).

⁵³K. Ronnmark, "WHAMP-Waves in homogeneous, anisotropic multicOMPONENT plASMAS" (Kiruna Geophys. Inst., 1982).

⁵⁴S. Kasahara, Y. Miyoshi, S. Yokota, T. Mitani, Y. Kasahara, S. Matsuda, A. Kumamoto, A. Matsuoka, Y. Kazama, H. U. Frey, V. Angelopoulos, S. Kurita, K. Keika, K. Seki, and I. Shinohara, *Nature* **554**, 337 (2018).